Eddy viscosity identification in the Ekman layer in North Western Mediterranean Sea.

Turboradar / Turbident / Urbarisq

C. Aldebert, M. Baklouti, D. Bourras, H. Branger, T. Caby, J.L. Devenon, D. Faranda, P. Fraunié, R. Fuchs, P. Garreau, G. Koenig, I. Pairaud, V. Rey, A. Sentchev, V. Shrira, S. Vaienti

Surface layer problem

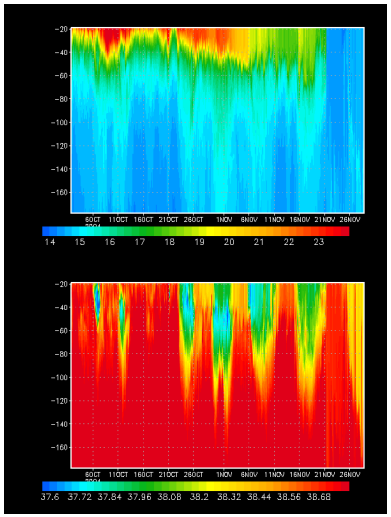

Gliders observations

(Testor et al, 2008)

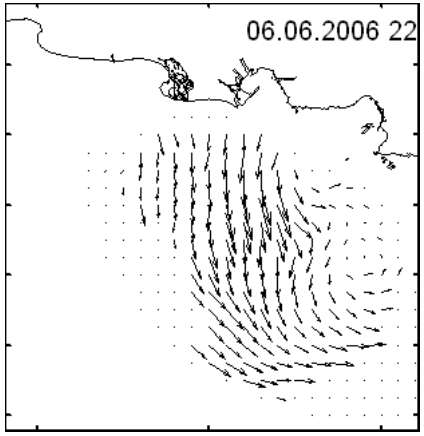

HF radars observations

(Forget & Shrira, 2015)

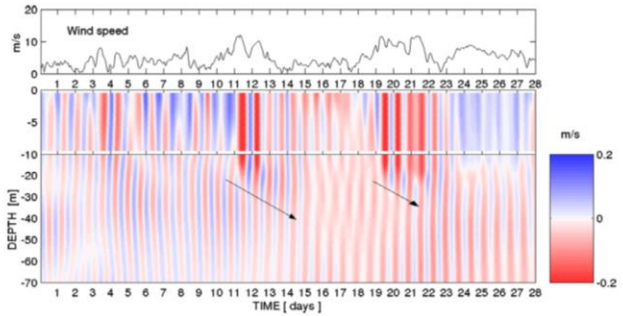

Fig. 19. Time evolution of the wind speed and of the vertical profile of the zonal current at 3.1°E/42.6°N during a 28 day period in summer, in a simulation with the GoL64 ocean circulation model driven with REMO forcing

Internal waves permitting models: summer 2008

Langlais et al, 2009, Schaeffer et al 2010

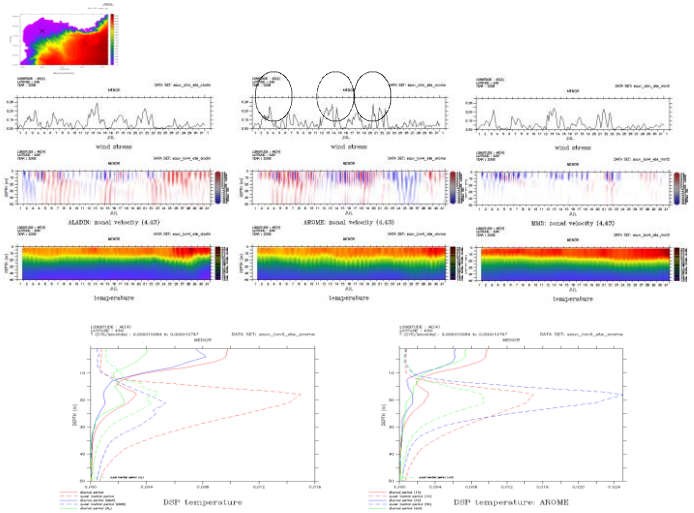

HF radars H current mapping

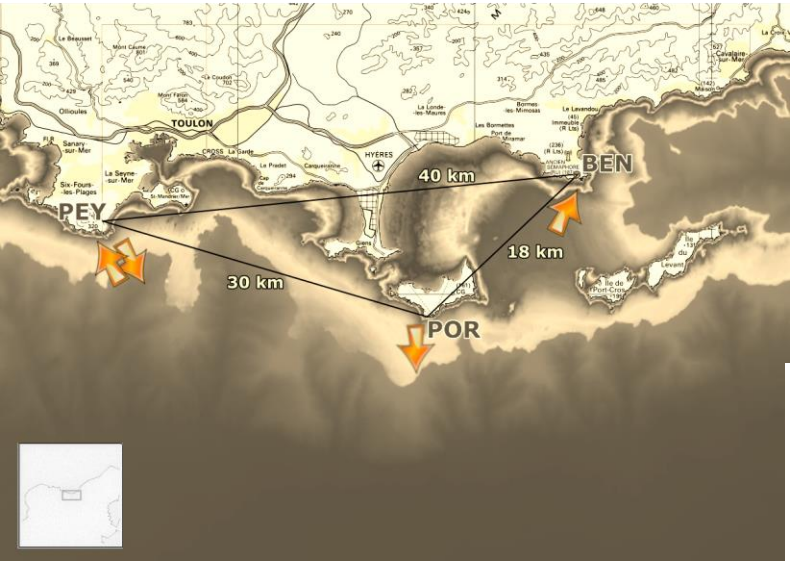

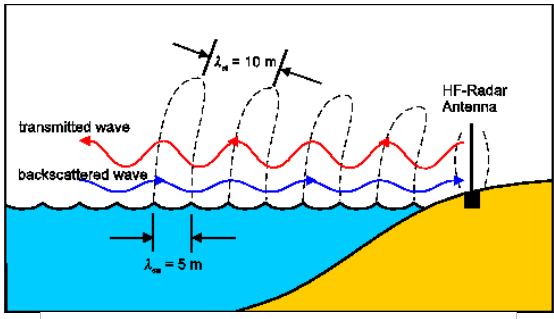

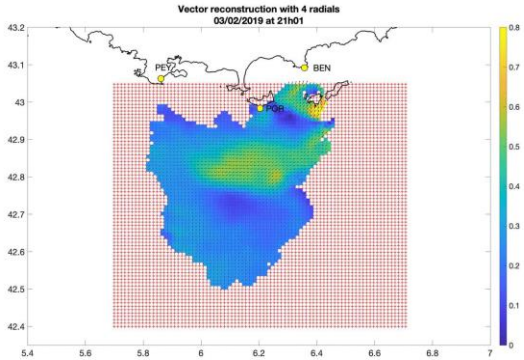

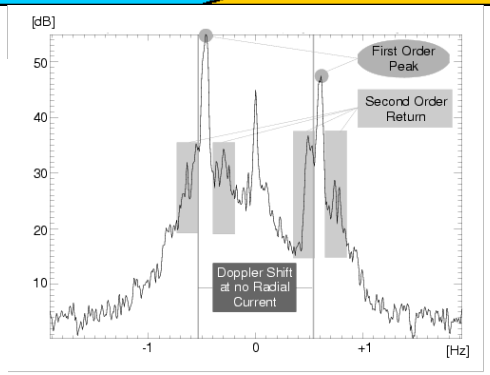

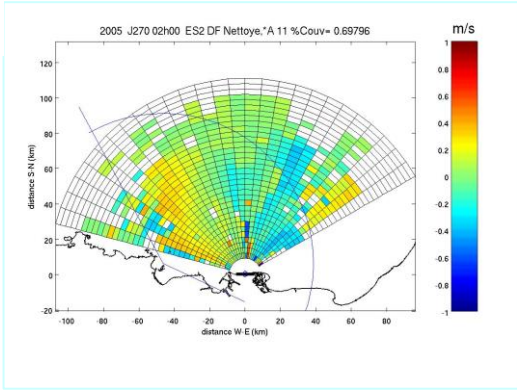

M.I.O. HF Radar team : C. A. Guérin (PR), C. Quentin(IR), A. Gramoullé (IE), D. Dumas(IE), B. Zakardjian(PR), A. Molcard (PR), M. Saillard (PR)

MOOSE / EU MARITTIMO SICOMAR PLUS / ANR TURBIDENT

SUBCORAD campaign 2013

Sentchev, Forget, Fraunié, 2015

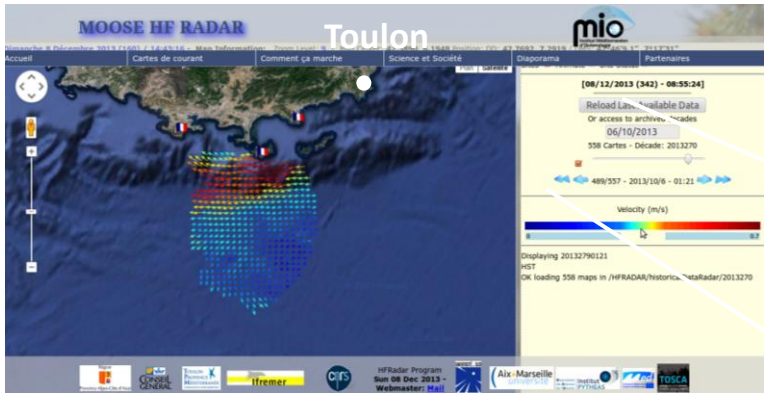

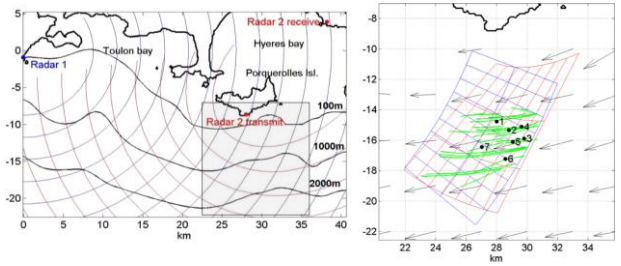

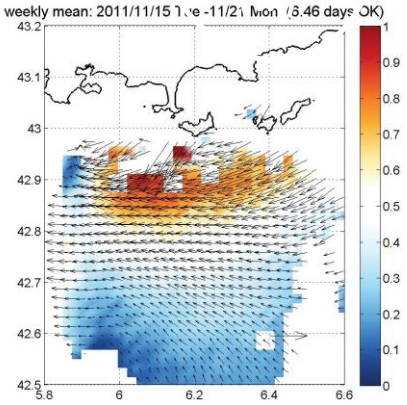

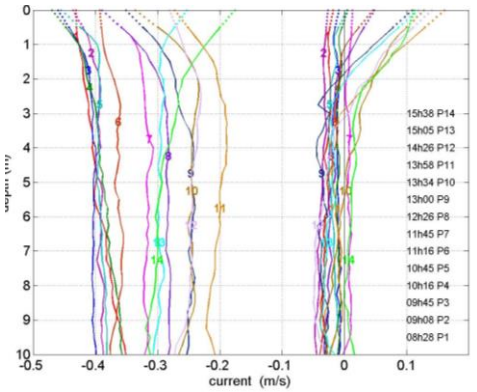

The Ekman (1905) solution

$$\frac{\partial u}{\partial t} - fv = \upsilon_t \frac{\partial^2 u}{\partial z^2} \qquad \frac{\partial v}{\partial t} + fu = \upsilon_t \frac{\partial^2 v}{\partial z^2}$$

- **Steady solution**

$$\begin{cases} U(z) = \text{sign}(f)\, U_c \sqrt{2} \exp\left(-\frac{z}{d_E}\right)\cos\left(\frac{\pi}{4} - \frac{z}{d_E}\right) \\ V(z) = U_c \sqrt{2} \exp\left(-\frac{z}{d_E}\right)\sin\left(\frac{\pi}{4} - \frac{z}{d_E}\right) \end{cases}$$

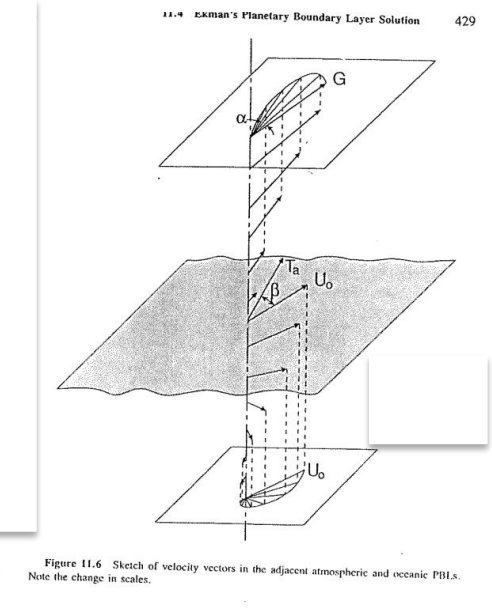

Figure 11.6 Sketch of velocity vectors in the adjacent atmospheric and oceanic PBLs. Note the change in scales.

- **unsteady solution**

$$\begin{cases} U(z,t) = \dfrac{2\,\tau_{sy}}{\rho_r\, d_E\, f} \displaystyle\int_0^{\tilde{t}} \frac{\sin(2\pi\zeta)}{\sqrt{\zeta}} \exp\left(-\frac{z^2}{4\pi d_E^2 \zeta}\right) d\zeta \\ V(z,t) = \dfrac{2\,\tau_{sy}}{\rho_r\, d_E\, |f|} \displaystyle\int_0^{\tilde{t}} \frac{\cos(2\pi\zeta)}{\sqrt{\zeta}} \exp\left(-\frac{z^2}{4\pi d_E^2 \zeta}\right) d\zeta \end{cases}$$

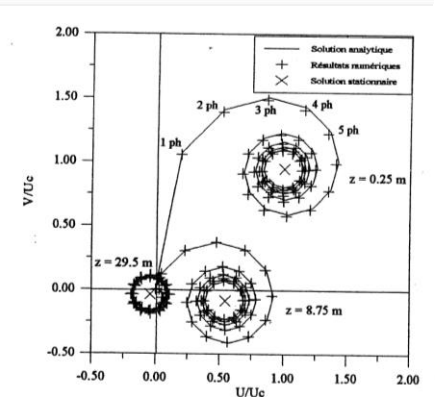

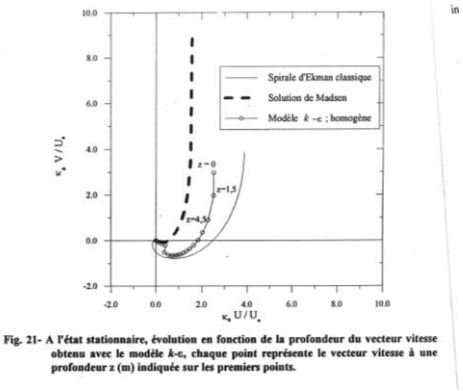

Fig. 21- A l'état stationnaire, évolution en fonction de la profondeur du vecteur vitesse obtenu avec le modèle *k*-ε, chaque point représente le vecteur vitesse à une profondeur z (m) indiquée sur les premiers points.

K-ε model (C. Verdier-Bonnet 1996, 1999)

Ekman layer inflectional Instability

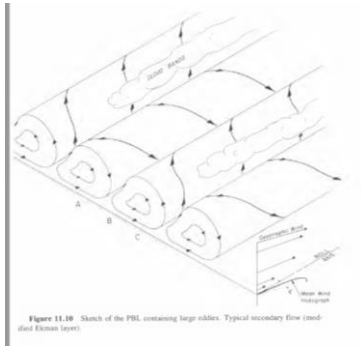

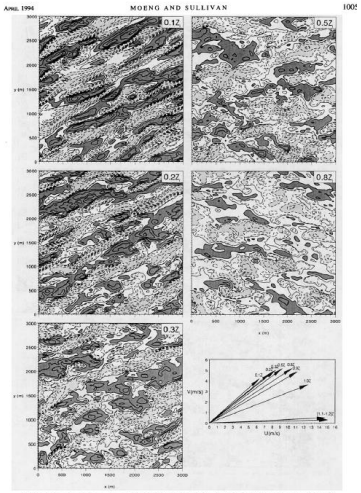

Moeng&Sullivan 1994

- **Ekman Spiral** (Ekman 1905, Gonella 1971, Madsen 1977, Lewis&Belcher 2004, Elipot&Gille 2009, Almelah&Shrira sub)
- **Stability analysis** (Faller 1965, Brown 1974, Leibovich & Lele, 1985)
- **LES** (Deardorff 1970, 1972, Mason & Thomson 1987, Moeng&Sullivan 1994, Zikanov et al, 2003, Sullivan&McWilliams 2010)
- **DNS** (Coleman, Ferziger, Spalart, 1990)
- **Observations PBL** (Le Mone 1973)
- **Observations Ocean** (Price et al 1987, 1999, Csanady 2001)

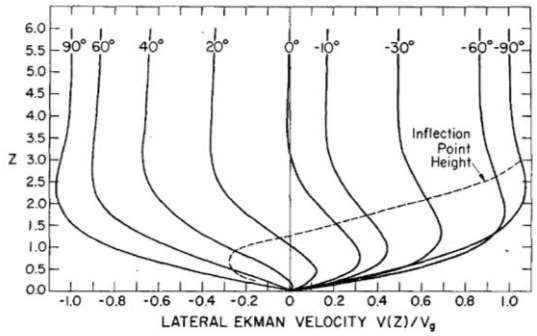

FIG. 1. Two-dimensional velocity profiles taken in vertical planes normal to the roll direction. The angle ϵ denotes the roll angle to the left of the geostrophic velocity. The height and velocity are given in increments of δ and V_g, respectively.

Brown 1972

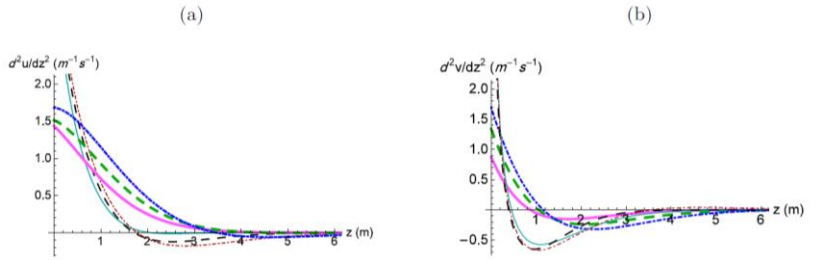

FIGURE 6. Second derivatives of the velocity profiles in two models of viscosity (the classical Ekman model (thick lines) and time-dependent viscosity model (thin lines)) at different times: $\tilde{t} = 2$ (solid lines), $\tilde{t} = 3$ (dashed lines) and $\tilde{t} = 5$ (dotted lines). (a) The second derivative of x-component. (b) The second derivative of y-component. The paramters: $\delta = 3$ hrs, $f = 10^{-4}s^{-1}$, $\nu_0 = 10^{-4}m^2s^{-1}$.

Almelah & Shrira sub

TURBIDENT campaign 2018

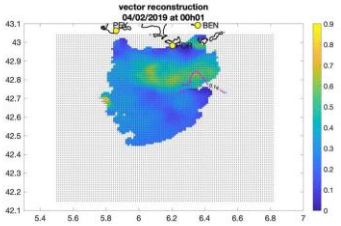

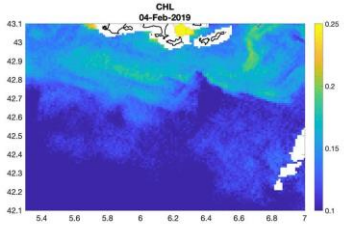

Dumas, Granoullé & Guérin

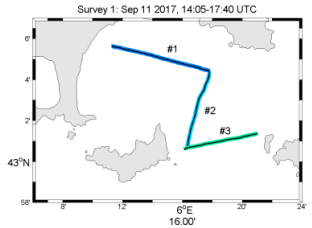

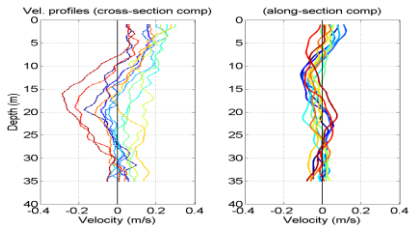

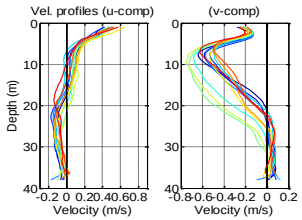

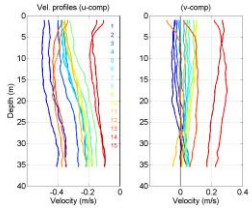

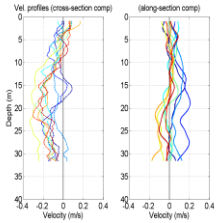

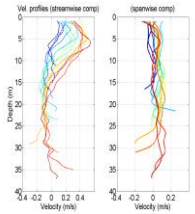

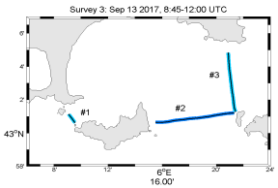

D. Bourras, H. Branger, A. Sentchev

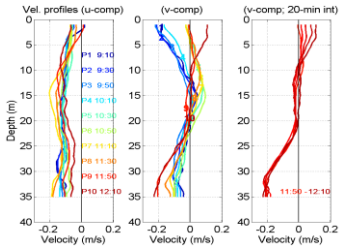

Eddy viscosity estimate

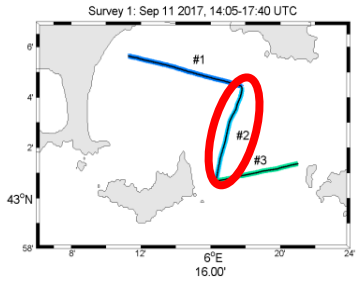

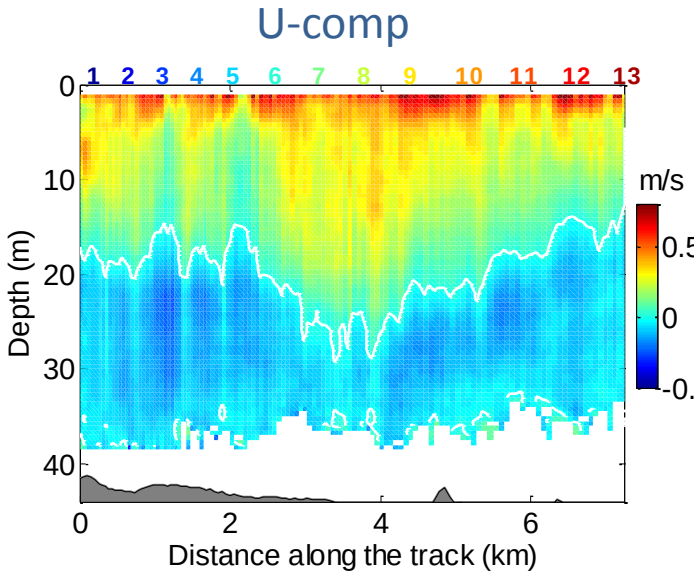

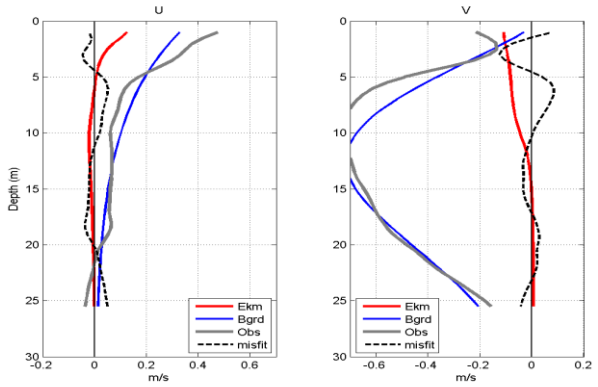

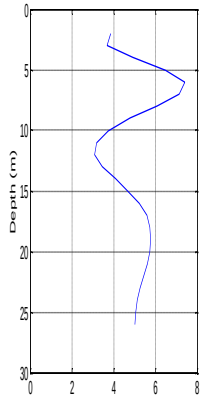

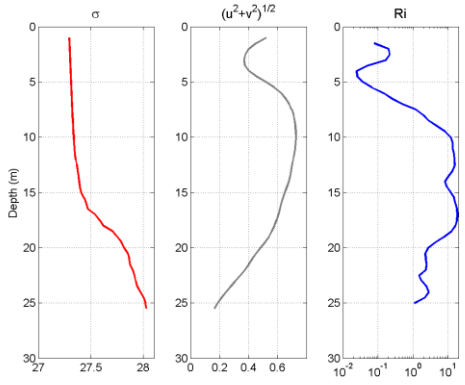

From 1 D Ekman model (A Sentchev)

Clément Aldebert, PhD
theoretical ecology, dynamical systems, statistics, oceanography
Postdoctoral Researcher
Mediterranean Institute of Oceanography
Aix-Marseille University
clement.aldebert@mio.osupytheas.fr

Parameter estimation of turbulent closure schemes in marine circulation models using Simultaneous Perturbation Stochastic Approximation method : a proof-of-concept.

Aldebert Clément(1), Devenon Jean-Luc(1), Fraunié Philippe(1), Pairaud Ivanne(2), Garreau Pierre(3)

(1) Mediterranean Institute of Oceanography, Aix-Marseille University, Toulon University, CNRS/IRD, France, (2) IFREMER Lerpac, La Seyne, France, (3) IFREMER LPOS, Brest, France

The operational problem

- predictions by numerical models of marine circulation strongly rely on the description of the sea-air interface
- difficult to acquire reliable data close to sea surface ⇒ practical challenge is to parameterize the turbulent closure schemes modelling the upper mixing layer
- TURBIDENT project aims to optimize turbulent closure schemes with a new well-suited data set from HF radars and AUV-mounted ADCP
- we use a new data assimilation method that has never been used for turbulent closure schemes optimization

Why this new method ?

- model derivatives with respect to the parameters to optimize are usually computed explicitly by an adjoint model that need to be developed and maintained
- the SPSA methods (Zhu & Spall, 2002) are based on a small number of model estimates (random parameter perturbations) to approximate at low numerical cost the derivatives by finite differences
- due to the random component, different methods (first and second-order, "modified") has been proposed to improve the procedure (numerical cost, stability)

Preliminary results

- we identified the most stable SPSA algorithm through theoretical examples of the surface layer
- ongoing tests for KPP model (link with interior domain, surface layer thickness)

Next steps

- stratified and/or unsteady situations
- sensitivity to sampling under realistic scenarios
- coupling SPSA with existing methods
- same work with k-ϵ model

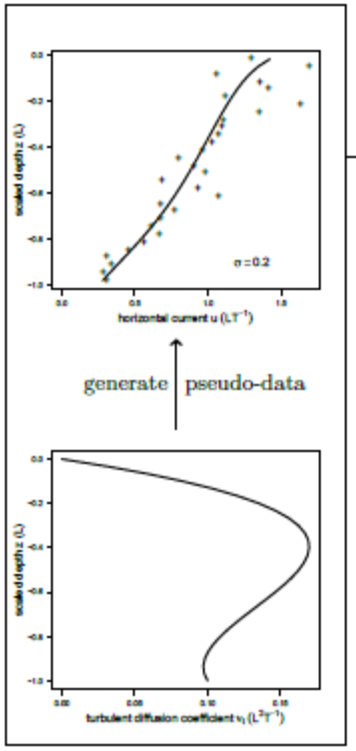

data on current profile

as constraints

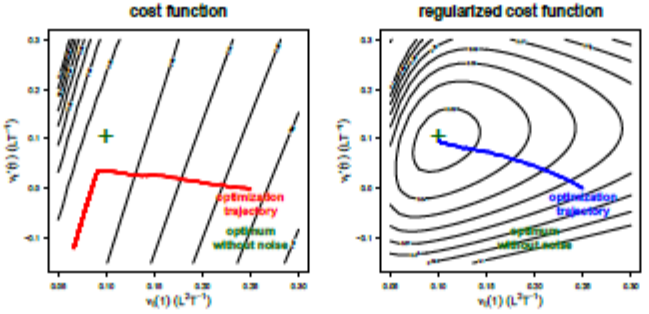

optimize parameters

to fit current profile

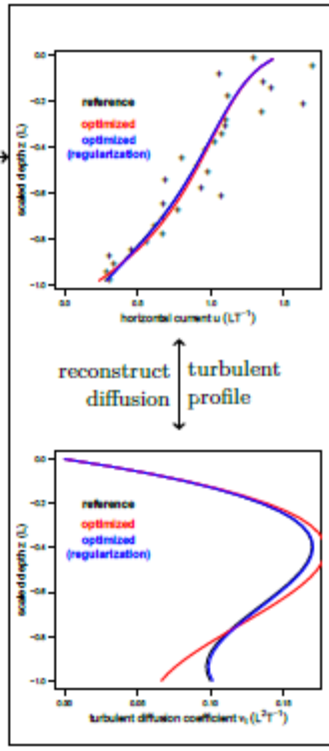

A steady-state example

Horizontal current (u) experiencing a turbulent diffusion (coefficient ν_t) along a scaled vertical axis ($z \in [0,1]$) :

$$\frac{\partial}{\partial z}\left(\nu_t(z)\frac{\partial u}{\partial z}\right) = 0, \text{ with the boundary condition } u(0) = u_0$$

Like in KPP model (Large *et al.*, 1994), $\nu_t(z)$ is taken as a third-order polynomial that depends on two parameters : its value $\nu_t(1)$ and derivative $\nu'_t(1)$ at the lower boundary (continuity with the interior profile in KPP model)

For reference parameters, we compute the ν_t and u profiles. The current profile is sampled at depths z_i and a random noise is added to generate pseudo-data :
$u_i^{obs} = \alpha_i u(z_i)$, $\alpha_i \sim \mathcal{N}(1, \sigma)$

Outline of SPSA methods

For a set of parameters to optimize θ (here $\theta = (\nu_t(1), \nu'_t(1))$), we define a cost function, here : $S(\theta) = \sum_{i=1}^{n} \left(u_i^{obs} - u_i^{mod}(\theta)\right)^2 / n$.

Starting from initial parameter values, each step involves :
1. simultaneous random perturbations : $\Delta\theta_i = \pm 1$ (equiprobability)
2. use $S(\theta \pm c\Delta\theta)$ to approximate the gradient by finite differences
3. optionnal : similar method for the Hessian (add 2 model runs)
4. use 2. and 3. to compute new parameter estimates (with checking)

For step 4., the modified SPSA method is the most stable :
$\theta^{new} = \theta - a\,\mathrm{grad}(S(\theta))$, where a is the mean of Hessian eigenvalues

One may include additionnal information in the cost function to regularize it, here (as example) :
$S(\theta) = \sum_{i=1}^{n} \left(u_i^{obs} - u_i^{mod}(\theta)\right)^2 / n + \lambda(\nu'_t(1) - \nu'^{obs}_t(1))^2$.

Large, W.G., McWilliams, J.C., Doney, S.C. 1994. Ocean vertical mixing : a review and a model with a nonlocal boundary layer parameterization. *Reviews of Geophysics*, 32(4), 363-403.

Zhu, X., Spall, J.C. 2002. A modified second-order SPSA optimization algorithm for finite samples. *International Journal of Adaptive Control and Signal Processing*, 16, 397-409.

Simultaneous Perturbation Stochastic Approximation method
1D TKE DyFaMed

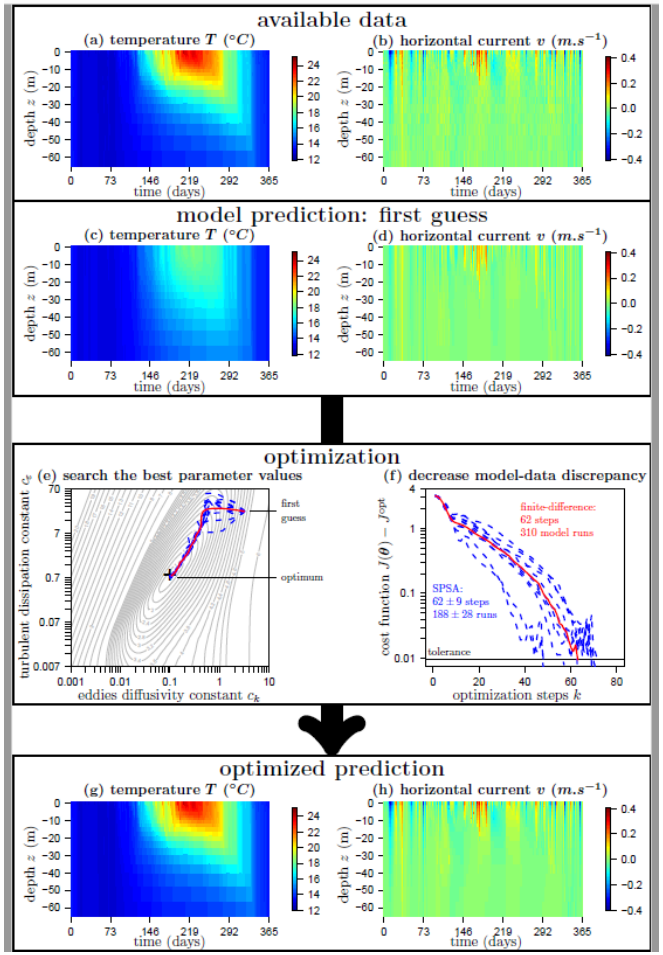

(Aldebert et al, submitted)

Sketch of the optimization problem from pseudo-data (a,b) and a model to attempt to describe data (c,d).

Model-data discrepancy is minimized by an optimization procedure that tunes the control parameters: evolution of parameters and map of the cost function (e), and corresponding decrease of the cost function J relatively to its value at optimum J opt in log-scale (f).

Here, one finite-difference gradient descent (red) and 10 SPSA runs (blue) starting from the same first guess are shown. The obtained parameter values lead to model predictions that are closer to observed data (g,h).

TKE closure model experiment

Aldebert et al sub

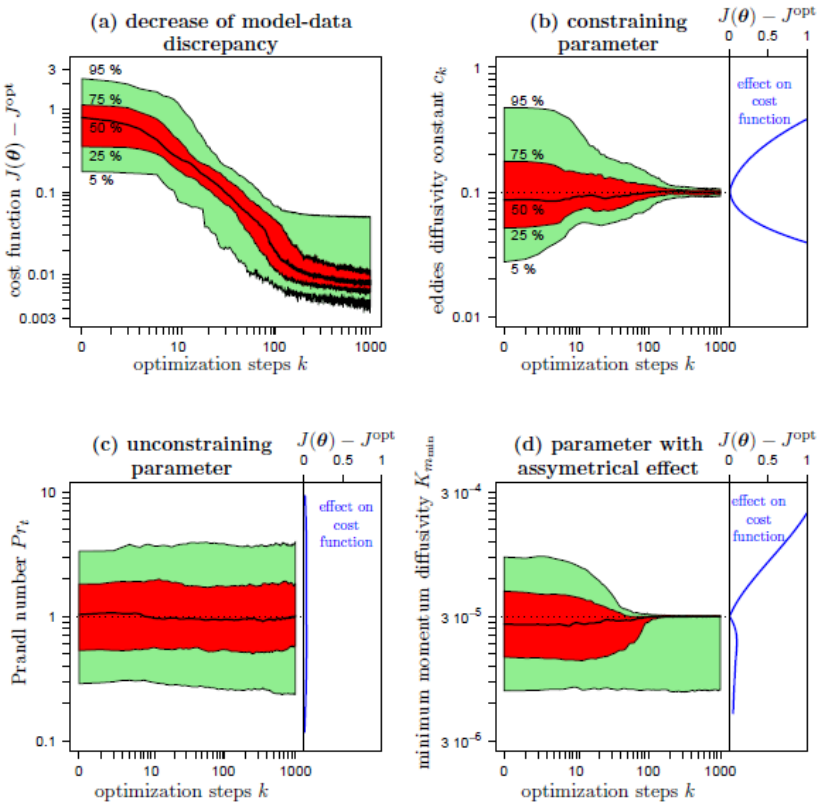

Figure 2. Statistics over 100 optimizations by SPSA of 8 parameters of the TKE model: decrease of the cost function $J(\boldsymbol{\theta})$ relatively to its value at optimum J^{opt} (a), and evolution of three parameter values (b-d) that summarize the three qualitative evolutions observed for the 8 parameters (complete figure with all parameters in Appendix). Note that all axes are in log-scale. Results are summarized by quantile intervals (5% – 95% in green, 25% – 75% in red) and the median (solid curve), and the optimal value to find for the parameters (b-d) is indicated by the dotted line. (b-d) The right-hand-side inset with a blue curve shows the sensitivity of the cost function to the parameter, estimated by a non-parametric local regression predicting the cost function value as a function of the parameter value, based on all the cost function evaluations performed during the 100 optimizations. A convex (flat) curve corresponds to a high (low)

Persistence extremal index method

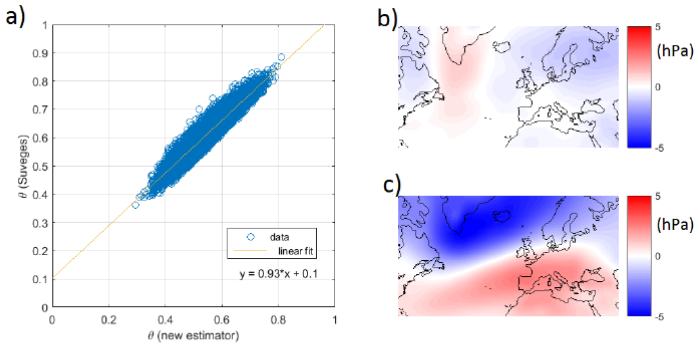

FIGURE 3. a) Scatter plot of $\hat{\theta}_{Su}$ (the Süveges estimator) vs $\hat{\theta}_5$ (the new estimator introduced in this work). Average map of the 5% sea-level pressure patterns such that the residual between $\hat{\theta}_{Su}$ and $\hat{\theta}_5$ are smaller than the 5% percentile (b) or larger (c) than the 95% percentile, for both taking as a threshold the 0.99-quantile of the observable distribution.

Caby, Faranda, Vaienti, Yiou, 2019

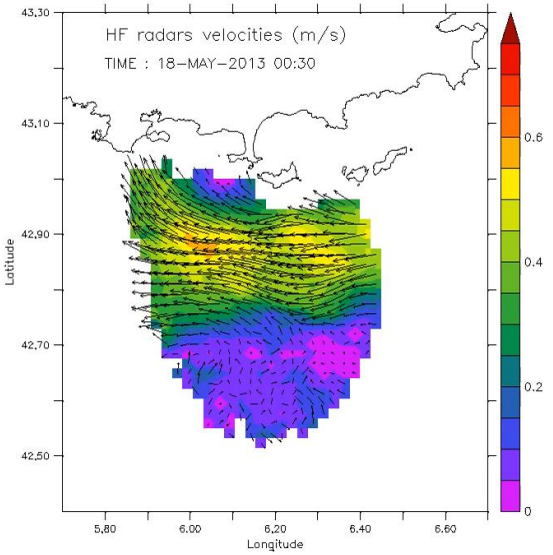

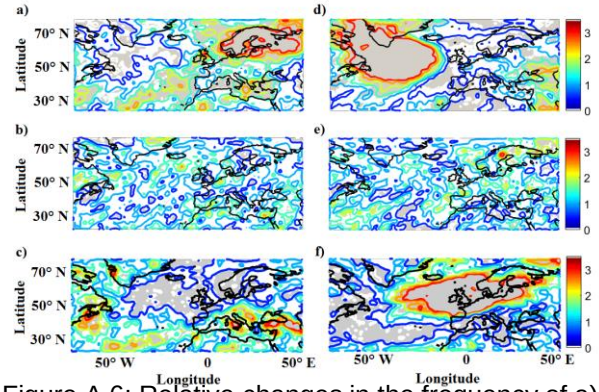

Figure A.6: Relative changes in the frequency of a), d) extreme cold; b), e) extreme wet and c), f) extreme 10m wind events for days with instantaneous dimension beyond the a-c) 0.98 and d-f) 0.02 quantiles of d in the ERA-Interim data. Contours start at 0, with an interval of 0.5; the grey shading shows statistically signicant changes. The maps in this gure are generated by MATLAB R2013a.

Faranda, Messori & Yiou 2019

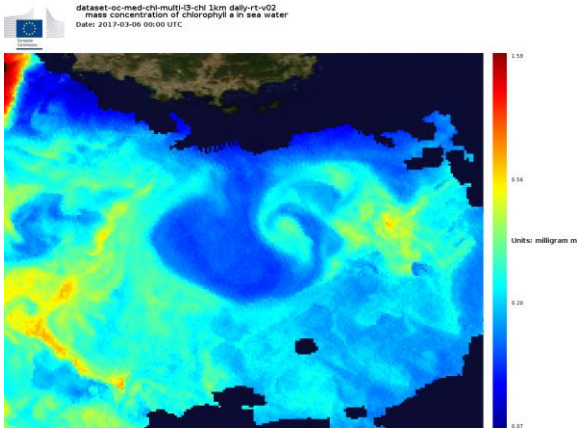

Dumas, Granoullé & Guérin

Conclusions

- 3D observations of the marine surface layer in microtidal sea have been started (2DH HF radars + 1V ADP/CTD profilers)
- Sensitivity of the surface mixing layer to eddy viscosity as function of 3D space and time has been investigated (still in a very limited number of situations)
- A fast method for Identification of parameters of turbulent closure models (TKE, KPP, etc) has been proposed (tests in progress)
- A data analysis approach based on dynamical systems has been proposed for sparse data sets to classify events (from rare to extreme) and provide statistics (persistence)
- Ekman model needs to be revisited for high resolution modeling (surface and internal waves, Stokes drift, Langmuir circulations, horizontal variations)

References

Aldebert C., Koenig G., Baklouti M., Fraunié P. and Devenon J.L. A fast and generic method to identify parameters in complex and embedded geophysical models: the example of turbulent closure in the ocean, *Geophys. Res. Letters*, submitted

Almelah R.B. and Shriraand V. I.Ocean response to varying wind in models with time and depth dependent eddy viscosity. J. Fluid Mech. Submitted

Bourras, D, H. Branger, G. Reverdin, L. Marié, R. Cambra, L. Baggio, C. Caudoux, G. Caudal, S. Morisset, N. Geyskens, A. Weill, and D. Hauser, 2014. A New Platform for the Determination of Air–Sea Fluxes (OCARINA): Overview and First Results. *J. Atmos. Oceanic Technol.,* 31, 1043-1062.

Bourras D. et al Air-sea Turbulent Fluxes from Six Experiments with data from a Wave-Following Platform. *JGR Oceans*, in revision

Caby,T., Faranda, D., Mantica G. , Vaienti S., Yiou P. Generalized dimensions, large deviations and the distribution of rare events *Physica* D submitted

Caby,T., Faranda, D., Vaienti S., Yiou P. On the computation of the extremal index for time series *Maths DS* submitted

Faranda D., Alvarez-Castro C., Messori G. 2019. The hammam effect or how a warm ocean enhances large scale atmospheric predictability *Nature communications* 10:1316

Langlais C., Barnier; B., Molines J-M, Fraunié P., Jacob D. and Kotlarski S. 2009. Evaluation of a dynamically downscaled atmospheric reanalysis in the prospect of forcing long term simulations of the ocean circulation in the Gulf of Lions. *Ocean Modelling* 30, 270-286.

Leredde Y., Devenon J.-L , I. Dekeyser. 1999. Turbulent viscosity optimized by data assimilation. *Annales Geophysicae*, 17, 1463-1477.

Leredde Y., Devenon J.-L , I. Dekeyser. 2000. Peut-on optimiser les constantes d'un modèle de turbulence marine par assimilation d'observations ? *C. R. Acad. Sci.,* Sciences de la Terre et des planètes,, 331:405-412.

Schaeffer A., Garreau P., Molcard A., Fraunié, P.Seity 2011. Y. Influence of high resolution wind forcing on the gulf of Lions hydrodynamic modelling, *Ocean Dynamics* vol61, 11, pp1823-1844.DOI: 10.1007/s10236-011-0442-3.

Sentchev A., Forget P., Fraunié P. 2017. Surface current dynamics under sea breeze conditions observed by simultaneous HF radar, ADCP and drifter measurements. *Ocean Dynamics*, 67, 3-4

Shrira V, Forget P. 2015, On the Nature of Near-Inertial Oscillations in the Uppermost Part of the Ocean and a Possible Route towards HF Radar Probing of Stratification, *J. Physical Oceanogr*., 45, 10, 2660-2678

Verdier-Bonnet C. , P. Angot, P. Fraunié, M. Coantic, 1999. Three dimensional modelling of coastal circulations with different closures, *J. Marine Systems*, vol 21, 1-4, 321-339,

Xing, A.M. Davies, P. Fraunié, 2004. Model studies of near-inertial motion on the continental shelf off northeast Spain : a 3D/2D model comparison study, 24p, *J.Geophys. Res.*, 109, C01017